ABSTRACT

BRYM, ADELINE JENNIFER. Base-Extracted Organic Matter Fluorescence Properties and Multivariate Statistics for Tracing the Sources and Transformations of Estuarine Particles. (Under the direction of Dr. Christopher L. Osburn).

Absorbance and fluorescence measurements were obtained and analyzed on base-extracted particulate organic matter (BEPOM) with an average extraction efficiency, based on total organic carbon, of 38%. BEPOM behavior and trends from August 2011-September 2012 in the Neuse River Estuary (NRE) were compared against single sampling events in the Charleston Harbor (CHS) and the inner Louisiana-Texas Shelf of the Gulf of Mexico (GOM) in July 2011 and July 2012, respectively. Spectral slope values, $S_{275\text{-}295}$, and the ratio of spectral slopes, S_R values, were driven by distinct structure in the UV-B region of the BEPOM absorption spectra. Fluorescence data from the three systems was used to fit a PARAFAC model for which six components were split-half validated. Four were of autochthonous production and two resembled humic substances. Organic carbon concentrations and stable carbon isotope values of BEPOM were measured for the NRE with most enriched values occurring mid-estuary. Finally, a Tucker's congruence coefficient (TCC) analysis was performed, comparing the components from this study to a previously published NRE PARAFAC model fit to BEPOM and colored dissolved organic matter (CDOM) fluorescence. Four components were identified as statistically similar between the two models. This study enhances the understanding of OM quality in BEPOM and CDOM and provides a stepping stone to tracing OM cycling between these two fractions of organic matter in estuaries.

© Copyright 2013 by Adeline Jennifer Brym

All Rights Reserved

Base-Extracted Organic Matter Fluorescence Properties and Multivariate Statistics for Tracing the Sources and Transformations of Estuarine Particles

by
Adeline Jennifer Brym

A thesis submitted to the Graduate Faculty of
North Carolina State University
in partial fulfillment of the
requirements for the degree of
Master of Science

Marine, Earth, and Atmospheric Sciences

Raleigh, North Carolina

2013

APPROVED BY:

Dr. David DeMaster	Dr. Astrid Schnetzer

Dr. Christopher L. Osburn
Committee Chair

DEDICATION

Made possible with help from family, friends, and mentors.

BIOGRAPHY

I grew up in Mansfield, Ohio and received my Bachelor's degree in Biochemistry/Molecular Biology from Wittenberg University in May 2010. At Wittenberg my passion for science and the ocean was strengthened with a minor degree in Marine Science which included a semester at the Duke University Marine Lab in Beaufort, NC.

In addition to taking classes and conducting research at NCSU, I was a teaching assistant for Oceanography and Earth System Science labs. I was also involved with the MEAS department and university's Graduate Student Association.

Immediate future goals after completion of a Master's degree include working a few years in industry and/or municipality. Long term goals include working in a non-profit environmental-focused organization to enhance and encourage public knowledge, appreciation, and stewardship in environmental issues.

ACKNOWLEDGMENTS

This work was supported by NCDENR 319 Grant 4443 (C.L.O., H.W.P.), the Strategic Environmental Research and Development Program Environmental Restoration grant (M.T.M., C.L.O.), the Lower Neuse Basin Association, (Neuse River Modeling and Monitoring Project, MODMON), (H.W.P.), the National Science Foundation (OCE 0825466, CBET 0932632) (H.W.P.) and the BP/Gulf of Mexico Research Initiative supporting consortium research (ECOGIG) administered by the University of Mississippi (GRIIDC Id R1.x132.134.0006) (K.Z).

Special thanks to the Osburn lab group; Jennifer Dixon, Molly Mikan, Luis Daniel Rojas-Jiménez, Lauren Hansel, Ruchi Bhattacharya, Kaitlin Tucker, Rich Taylor, Luke Sachsenmaier and especially Dr. Chris Osburn without whom this work would not be possible.

TABLE OF CONTENTS

LIST OF TABLES vi
LIST OF FIGURES vii

INTRODUCTION 1
METHODS 5
RESULTS 10
DISCUSSION 16
CONCLUSION 23

FIGURES 26
TABLES 38

REFERENCES 43
APPENDIX 48

LIST OF TABLES

Table 1 Site information 39
Table 2 PARAFAC excitation and emission wavelengths 40
Table 3 NRE geochemical data.....41
Table 4 TCC Analysis.....42

LIST OF FIGURES

Figure 1 Study sites....26
Figure 2 NRE absorption....27
Figure 3 CHS and GOM absorption....28
Figure 4 Spectral slope and S_R....29
Figure 5 $S_{275-295}$ pre and post correction....30
Figure 6 S_R pre and post correction....31
Figure 7 PARAFAC model....32
Figure 8 NRE geochemical and chlorophyll a trends....33
Figure 9 GOM Fmax Plot....34
Figure 10 NCG PCA....35
Figure 11 NRE PCA....36
Figure 12 Sample EEMs....37

Figure A.1 Osburn et al. 2012 PARAFAC model....49

INTRODUCTION

Optical properties of organic matter (OM) play an important role in aquatic ecosystems by controlling the availability and spectral quality of light in the water column (Jerlov 1976; Del Vecchio and Blough 2002; Hargreaves 2003). Photochemical reactions of light-absorbing compounds also directly affect aquatic biogeochemistry by producing inorganic carbon, mediating redox reactions of trace metals and influencing air-sea exchange of trace gases (Vahatalo and Zepp 2005). In coastal environments (estuaries to the inner shelf of the coastal ocean), the majority of light attenuation is controlled by the fraction of dissolved organic matter (DOM) that absorbs light and the corresponding fraction that fluoresces light, which are known as CDOM and FDOM, respectively.

The chemical composition of organic matter in coastal environments is complex, being comprised of perhaps thousands of compounds. Within coastal environments, these compounds can be partitioned into allochthonous and autochthonous sources of organic matter. Allochthonous compounds are delivered to coastal environments (e.g., through estuaries) from their catchments, whereas autochthonous sources are formed within coastal environments (predominantly from primary and secondary production). Allochthonous OM is dominated by humic substances, which are poorly characterized aggregates of individual compounds, high in molecular weight and generally existing as polymeric units (Sleighter and Hatcher 2007). In contrast, autochthonous compounds generally are non-humic in that they tend to retain their chemical identity within a mixture. Humic substances are further defined by their solubility: humic acids are soluble only in base while fulvic acids are soluble

in acid and in base (Stevenson 1994; Santín et al. 2009). Transformations of OM may occur within coastal environments, which may alter its chemical identity. Important processes are photochemical bleaching, bacterial degradation, and autochthonous production by phytoplankton and microbes (Rochelle-Newall and Fisher 2002; Romera-Castillo et al. 2011).

The use of multivariate statistical tools, such as parallel factor analysis (PARAFAC) and principal component analysis (PCA), to statistically decompose individual fluorescing excitation and emission matrices (EEMs) and model the prevalent fluorescence spectra, has dominated the literature in the past few years (Stedmon et al. 2003; Kowalczuk et al. 2009; Fellman et al. 2011). This technique is an inexpensive and efficient means of quickly estimating organic matter source and transformation. FDOM studies have ranged from using mesocosms to understand the influence of microbes and phytoplankton, tracing various allochthonous sources in coastal waters, to modeling its global distribution (Urban-Rich et al. 2006; Osburn and Stedmon 2011; Jørgensen et al. 2011).

Measurements of optical properties of POM have been limited to obtaining absorbance values directly off a saturated filter (Vernet and Whitehead 1996). POM often is operationally defined as organic matter greater than 0.7 μm and its collection involves filtration onto a glass fiber filter. A recent method involving base extraction of organic matter has raised the opportunity of conducting fluorescence spectroscopy on POM (Osburn et al. 2012). The method has its origins in studies of alkaline extracts of soils and sediments (e.g., Santín et al. 2009). It is unknown how base-extracted POM (termed BEPOM)

fluorescence behaves in coastal environments. It is expected that BEPOM fluorescence and absorbance properties behave similar to CDOM in similar systems.

In this study, BEPOM optical properties were compared for three coastal environments. The main focus of this study was the Neuse River Estuary (NRE) in eastern North Carolina. The NRE is a shallow, river and wind dominated system that flows into Pamlico Sound, the second largest estuarine complex in the United States. The Neuse River watershed covers an area of approximately 16,000 km^2, flowing through wetlands, forests, and heavy agriculture (U.S. Environmental Protection Agency [EPA] 1999; U.S. Department of Agriculture [USDA] 2001). Water quality and clarity has been a concern for this highly eutrophic and storm sensitive system (Paerl et al. 1998; Burkholder et al. 2006). Monthly surface samples were collected between August 2011- September 2012 as part of the Neuse River Estuary Modeling and Monitoring Program (MODMON).

The second coastal environment studied was Charleston Harbor (CHS) in South Carolina. This estuary is a harbor shelf environment dominated by marine processes, yet having three small riverine inputs (Ashley, Cooper, and Wando). CHS lies in the extensive southeastern coastal plain of the United States (colloquially known as "the Low Country") and its catchment is dominated by substantial *Spartina* marshes and tidal creeks (Wiegert and Freeman 1990).

The third coastal environment studied was in the Gulf of Mexico (GOM) with samples collected in the inner Louisiana-Texas Shelf, east of the Mississippi River plume. Globally, the Mississippi River has the third largest drainage basin area in the world and

sixth largest freshwater discharge accounting for around 60% of total suspended matter transported from the continental United States (Milliman 1991; Presley et al. 1980). The LTX site was influenced both by the Mississippi River plume and by marine processes. Samples collected from the CHS and GOM each occurred during one time sampling events and were compared to the synoptic study of the NRE.

This study explored BEPOM absorption and fluorescence properties across three estuarine environments. With a majority of the samples from the NRE, we fit two PARAFAC models of EEM fluorescence to distinguish the influence of this system from the CHS and GOM. The five components resolved from a PARAFAC model using only NRE data (NRE-PARAFAC model), were spectrally similar to five of the six components resolved in a second PARAFAC model containing data from all three sites (NGC-PARAFAC model). The NGC-PARAFAC model was analyzed to determine BEPOM source and trends in each system and examined against known CDOM trends. Optical measurements, including spectra slope and fluorescence components, were also analyzed against geochemical proxies of base-extracted particulate organic carbon (BEPOC) concentrations and δ^{13}C-BEPOM. The results of this study improved the understanding of organic matter cycling in coastal waters by using BEPOM absorbance and fluorescence to evaluate POM quality in these important ecosystems.

METHODS

Study sites

Surface samples (n=168) were collected on a monthly basis from August 2011 to September 2012 from the Neuse River Estuary, NC (NRE) and the Trent River (TR), a tributary located near the river mouth (Fig. 1a). Samples from the thirteen stations were collected over the 70 km transect. Station names increase from NRE0 to NRE180 as the sites move downstream. Bimonthly samples were included for August 2011, September 2011, and March 2012. NRE samples were collected in clean polyethylene bottles and shipped on ice to the home laboratory at NC State University. Estuarine particles were collected onto a 0.7 μm GF/F filter and stored frozen until further analysis.

Depth profiles were taken from seven stations in Summer 2011 from the Charleston Harbor, SC (CHS) (Fig. 1b). Sample sites included three rivers, the Ashley, the Cooper, and the Wando, inside the harbor, and approximately 11 km off shore in the South Atlantic Bight (SAB). Gulf of Mexico (GOM) sampling also included depth profiles (Fig. 1c). Samples were collected in Summer 2012 from three sites located off the continental shelf. CHS and GOM samples were filtered on site and frozen GF/F filters for particulate and chlorophyll a (CHS) analysis were transported to NC State University. Samples of the benthic bottom boundary layer (nepheloid) were pumped into collection vessels through an intake funnel affixed to a metal frame ca. 15 cm above the sediment (Pohlman et al. 2002). Silicone tubing and a Teflon pneumatic pump was used in this apparatus.

Base extraction

POM material was extracted from the filter into 0.1 *N* sodium hydroxide (NaOH) for 24 hours at 4° C, following Osburn et al. (2012). The basic solution was neutralized with concentrated hydrochloric acid (HCl) and filtered through a 0.2 µm PES filter prior to measurement of absorbance and fluorescence on Varian Cary 300 and Eclipse instruments, respectively.

Absorbance spectra were measured from 220-800 nm. Samples with raw absorbance greater than 0.4 at 240 nm were diluted. All samples were blank-corrected against a neutralized NaOH control. Absorbance measurements were converted into Napierian absorption coefficients (m^{-1});

$$a(\lambda) = a(\lambda_0)e^{S(\lambda_0-\lambda)} \quad (1)$$

where *a* is the absorption coefficient at reference wavelength, $\lambda_{0,}$ and *e* is the exponential of the spectral slope at a given range (Bricaud et al. 1981). Spectra slopes used in this study were between 275-295 nm ($S_{275\text{-}295}$) and 350-400 nm ($S_{350\text{-}400}$). Slope ratios (S_R) of the two spectra slopes were also calculated (Helms et al. 2008).

Fluorescence excitation-emission matrices (EEMs) were measured at excitation wavelengths 220-500 nm with 5 nm excitation slits and the corresponding emission wavelengths were measured between 240-600 nm with 5 nm emission slits. Fluorometer voltage measurements ranged from 800-950 nm at a scan rate of 4800 nm min^{-1}. Integration time was 0.025 s. Fluorescence measurements were corrected for inner-filter effects,

calibrated against the instrument's Raman signal, and standardized to quinine sulfate units (ppb QSE) (Lawaetz and Stedmon 2009). Additional corrections were included to account for volume filtered, dilutions, and absorbance path length.

Absorption spectra corrections

Additional corrections were applied to remove structure present in the UV region in BEPOM absorption spectra. To mimic featureless exponential decay exhibited in CDOM absorption, BEPOM absorption values between 280-301 nm were removed. A non-linear function was then applied to interpolate the excised data. $S_{275\text{-}295}$, $S_{350\text{-}400}$, and S_R of the natural log of the corrected absorption values were then recomputed and compared to the original values and previously published CDOM values.

BEPOC and δ^{13}C-BEPOM calculations

BEPOC and δ^{13}C-BEPOM isotopes were obtained on a Delta V plus, Isotope Ratio Mass Spectroscopy (IRMS). Prior to runs, BEPOM was diluted with 10 ml Millipore Milli-Q water and acidified to pH 2 with 85% phosphoric acid (H_3PO_4). Samples were blank corrected against 0 mgC L^{-1} potassium hydrogen phthalate (KHP). A KHP linear regression curve (0, 1, 5, 10 mgC L^{-1}) was used to calculate BEPOC values. Final BEPOC values accounted for Milli-Q water dilutions and initial filtration volume.

A mass balance equation was used to correct δ^{13}C values against the NC State University CO_2 reference gas and the international reference;

$$\delta^{13}C = \left[\frac{{}^{13}C /{}^{12} C_{sample}}{{}^{13}C /{}^{12} C_{std}} - 1 \right] * 1000 \qquad (2)$$

where all $\delta^{13}C$ values are relative to PDB standards in ‰ notation (Matson and Brinson 1990).

Chlorophyll a

Chlorophyll a was measured on samples from CHS following EPA Method, 446.0, which uses the trichromatic equation (Arar 1997). Filters were ground and extracted in a 90:10 acetone:water solution in the dark for 2-24 hours at 4°C before absorbance was measured. All samples were blank corrected against the acetone:water solution.

NRE in situ chlorophyll concentrations were obtained from a flat Li-Cor sensor (UWQ-PAR6067) coupled with an YSI 650 MDS Multi-parameter Display System datalogger. GOM in-situ chlorophyll concentrations were from a Wet Labs ECO Chlorophyll Fluorometer. All chlorophyll a values were reported in micrograms per liter.

Statistical modeling

Parallel Factor Analysis (PARAFAC) modeling was completed in the MATLAB computing environment (Mathworks, Inc., Natick, MA) with the DOMFluor toolbox (Stedmon and Bro 2008). PARAFAC is a mathematical tool that statistically decomposes multi-way data into a set of three linear terms and a residual array to produce robust, non-bias models using;

$$x_{ijk} = \sum_{f=1}^{F} a_{if} b_{jf} c_{kf} + \varepsilon_{ijk}, i = 1,.,I;\ j = 1,.,J; k = 1,.,K; \quad (3)$$

In this chemometrics approach, x_{ijk} is the intensity of fluorescence for the *i*th sample at emission wavelength *j* and excitation wavelength *k*. *F* defines the number of components in the model. Parameter *a* is directly proportional to the concentration of the *f*th analyte in

the *i*th sample. The emission spectrum is represented by parameter *b* as b_{if} is linearly related to the fraction of absorbed energy emitted as fluorescence (fluorescence quantum efficiency) of the *f*th analyte at emission wavelength *j*. Parameter c_{kf} represents the excitation spectrum with a linear relationship to the specific absorption coefficient at excitation wavelength *k*. Lastly, the variability of the residual matrix not explained by the model is represented by e_{ijk}. Model calculations are based on minimizing the sum of square residuals with an alternating least squares algorithm (Bro 1997; Stedmon et al. 2003; Kowalczuk et al. 2009). Maximum fluorescence intensities of each component (Fmax) was calculated by multiplying the fluorescence concentration score in every sample EEM with the excitation and emission maxima for each component and reported in Raman Units (R.U).

Initially two models were derived. The NRE-PARAFAC model comprised of EEMs from the NRE (n=183). A normalization parameter was applied to EEMs from the NRE, CHS, and GOM (NCG) before creating the NCG-PARAFAC model (n=217). The models were split-half validated by dividing the data array into two halves and creating separate matching PARAFAC models. Random initialization confirmed the best fit by modeling the sum of squared error.

The PLS toolbox (Eigenvector, Inc.) was used to create Principal Component Analysis (PCA) to examine the loadings and leverages from the PARAFAC results. Additional parameters in the model included: chlorophyll a, salinity, $S_{275\text{-}295}$, BEPOC, stable carbon isotopes, and dissolved oxygen.

RESULTS

BEPOM absorption spectra variability

Absorption spectra from the NRE show variability within the estuary and with season (Fig. 2). The low salinity, riverine end-member (NRE0) exhibited a shallow peak around 280 nm while mid-salinity and high salinity stations exhibited absorption spectra with noticeable structure: broad peaks between 280-320 nm and around 400 nm. Seasonal variability in the absorption spectra was observed. For example, BEPOM absorption intensity was greatest at station NRE0 and decreased with increasing salinity in September 2011 and March 2012 (Fig 2a; Fig. 2c). In February 2012 and September 2012, however BEPOM absorption was greatest at the mid-estuary, station NRE60 (Fig. 2b; Fig. 2d).

Overall, spectral peaks were identified in the CHS and GOM, but the intensities of BEPOM absorption spectra were lower than those from the NRE (Fig. 3). Freshwater influenced stations (e.g. CHS0 and CHS17), exhibited shallow peaks in the UV. Intensity and broadness of a spectral peak was more pronounced in more marine influenced stations.

Outside of Charleston Harbor, on the shelf of the SAB, the absorption spectra exhibited minimal change and distinct peaks were observed throughout the 18 meter water column (Fig. 3a). The strongest absorption at this shelf site was at 10 m. BEPOM absorption spectra from samples on the inner shelf of the GOM (Sta. 2) were similar to the inner shelf of the SAB (Fig. 3b). The maximum absorption was measured at 16 meters below sea surface and prominent absorption peaks were clear in the 0 and 16 m samples.

These peaks were far less pronounced in the deeper samples of the inner shelf collected at 55 m and 132 m, respectively.

Changes to BEPOM spectral slope values

In estuarine environments, spectral slope (S) values can represent, for CDOM, usually distinction between end member as S values tend to increase with salinity (Stedmon and Markager 2003; Helms et al. 2008). For the NRE, mixing is between the Neuse River and the Pamlico Sound. Figure 4a shows the change in BEPOM $S_{275\text{-}295}$ and $S_{350\text{-}400}$ values we measured down the estuary, across the salinity gradient for all NRE samples. $S_{275\text{-}295}$ values increased in absolute magnitude with increasing salinity, ranging from 0.010 to 0.062 nm^{-1}. CHS and GOM $S_{275\text{-}295}$ values also fall within said range (Table 1). The positive linear relationship between $S_{275\text{-}295}$ and salinity has been observed for CDOM in the Delaware Bay Estuary and in the Mississippi River plume, but at lower magnitudes (Helms et al. 2008; Fichot and Benner 2012). Absolute BEPOM $S_{350\text{-}400}$ values ranged from 0.00460 to 0.0208 nm^{-1} but did not exhibit a clear trend with salinity.

Changes in S_R values with salinity in the NRE were plotted for select months that show contrasting trends in the behavior of this parameter (Fig. 4b). A slight decrease in S_R as a function of salinity was observed in September 2011 and all S_R values were <1. In contrast, February 2012, March 2012, and September 2012 all exhibited steep increases in S_R values with values ranging from around 1 to 4. The pattern in BEPOM S_R values tended to follow the pattern in $S_{275\text{-}295}$ values as opposed to $S_{350\text{-}400}$ values. Thus, it appears the S_R

values calculated for BEPOM in the NRE largely are controlled by the slope region of 275-295 nm. Similar behavior was observed for CDOM S_R values (Helms et al. 2008).

Effect of BEPOM absorption peaks on NRE spectral slope values

It was clear that the presence of the intermittent peaks in the NRE BEPOM absorption spectra near 280 nm and near 400 nm likely influenced $S_{275\text{-}295}$ and $S_{350\text{-}400}$ values, and thus resulting in the relatively large S_R values we observed (Fig. 4b). Therefore, we wanted to test the effect of the peaks on S_R values. To do so, BEPOM absorption spectra were re-processed to remove the broad peak from each spectrum, when it was present. We performed this analysis on the NRE data set because we had most observations from said system. First derivatives of the BEPOM absorption spectra were calculated and indicated that the peak generally occurred between 240 and 400 nm, ca. 285 nm (Fig. 2). Next, a nonlinear fit of the resulting absorption values was applied to re-populate each absorption spectrum with estimated values calculated by interpolation, based on using Equation 1 to predict the fit parameters. Finally, new $S_{275\text{-}295}$, $S_{350\text{-}400}$, and S_R values were computed on the peak-corrected spectra. These values were then compared to pre-corrected values.

Correction of the absorption spectra by removing the broad peak resulted in lower $S_{275\text{-}295}$ values than without the correction (Fig. 5a). However, a positive linear relationship was found between $S_{275\text{-}295}$ from the original absorption spectra and $S_{275\text{-}295}$ from the spectra corrected for BEPOM absorption structure (Fig. 5b). The post-corrected values also clustered together more tightly in a generally linear increase with salinity. Thus, $S_{275\text{-}295}$ values calculated via either method increased with increasing salinity; however, the

magnitude of the difference between the two $S_{275-295}$ values for a given sample increased down the estuary (Fig. 5a). This resulted in a linear correlation between pre- and post-corrected slope values but an off of ~0.005 nm^{-1} (Fig 5b). A low correlation (correlation coefficient, *R*, = 0.45) was observed between the original and peak corrected S_R values, which is apparent when the pre- and post-corrected S_R values were plotted together as a function of salinity (Fig. 6). This likely was driven by both the magnitude of the broad peak and the low signal at higher wavelengths, which interfered with the non-linear fit of the excluded absorption data.

PARAFAC modeling of BEPOM in estuaries

PARAFAC models were fit to the NRE data separately (NRE-PARAFAC model) and to the NRE, CHS, and GOM data collectively (NCG-PARAFAC model). Five components were validated in the NRE-PARAFAC model and six components were validated in the NCG-PARAFAC model. In the NRE-PARAFAC model, the five components appeared very similar to five of the six components in the NCG-PARAFAC model (Table 2). The components were determined in rank order of increasing explanation of variability. Hence, similar components were ranked differently between the two models. Further analysis will only regard the NCG-PARAFAC model (Fig. 7).

Component 1 excitation wavelength maxima was at 245 nm and 305 nm with emission wavelength around 410 nm, and strongly resembles ubiquinone, the oxidized form of NADH (Fig. 7a; Cory and McKnight 2005; Li et al. 2011). This fluorescence component also has been previously identified in DOM from a eutrophic estuary with strong urban and

agriculture land use in its catchment (Fellman et al. 2011). Moreover, the NADH-like component was prevalent in a combined POM-DOM PARAFAC model of the NRE (Osburn et al. 2012). A broad excitation with a maximum around 240 nm was observed in component 2 (Fig. 7b). The corresponding emission was greater than 400 nm, similar to terrestrial fulvic acids (Senesi et al. 1989). Component 3 had excitation/emission maximas at 275 nm and 334 nm respectively (Fig. 7c). The pattern strongly resembled tryptophan, reflecting recent biological production (Rochelle-Newall and Fisher 2002; Stedmon and Markager 2005; Romera-Castillo et al. 2010). Component 4 exhibited dual excitation at 250 and 360 nm with a corresponding emission at 440 nm (Fig. 7d). This signal has been identified in other eutrophic systems, but not in coastal waters (Murphy et al. 2008; Jørgensen et al. 2011). Protein-like peaks also were identified in Component 5, with double excitation peaks at 240 nm and 295 nm and an emission peak at 334 nm (Fig. 7e; Coble 2007). A similar fluorescence component, although slightly blue shifted, was modeled on DOM collected in the North Sea-Baltic Sea mixing zone (Osburn and Stedmon 2011). Component 6 was unique to the NCG-PARAFAC model with primary excitation maxima near 340 nm, secondary excitation <240 nm, and an emission maximum at 440 nm (Fig.7f; Table 1).

BEPOM OC concentrations and $\delta^{13}C$ values

BEPOC concentration and δ^{13}C-BEPOM values were measured only on a subgroup of the NRE dataset (n=136 and n=86 respectively; Table 3). BEPOC concentrations were also compared to POC concentrations and the extraction efficiency of BEPOM computed.

The extraction of organic carbon in BEPOM from total POM averaged around 38% ranging from 5% to 95%. Extraction efficiency was not influenced by station or seasonality.

BEPOC and δ^{13}C-BEPOM values showed very dynamic trends in the NRE. Figure 8 represents BEPOC concentrations, chlorophyll a, and δ^{13}C-BEPOM values for February, March, and August 2012. BEPOC behaved similarly between the three months (Fig. 8a). The average value at the terrestrial end-member was ~200 μgC L^{-1}. BEPOC values peaked in the mid-estuary with the greatest value at NRE100 in March 2012 (2560 μgC L^{-1}). Concentrations continued to decrease in February and March to slightly below 300 μg/L. August 2012 was an exception with a sharp increase at the marine end-member, sta. NRE180.

δ^{13}C-BEPOM values ranged between -32 and -23‰ (Fig. 8c). These values reflected the high influence of isotopically-depleted terrestrial organic matter to the NRE as well as some in situ production (Matson and Brinson 1990). A slight depletion in δ^{13}C-BEPOM values occurred in the first 20 km of the estuary for the three sampling dates. The stable carbon isotope values became enriched mid-estuary. This enrichment corresponded with stations having the highest chlorophyll a concentrations (Fig. 8b). In the lower estuary, δ^{13}C-BEPOM values were depleted slightly and chlorophyll concentrations decreased relative to mid-estuarine values.

DISCUSSION

Base-extraction of POM and the subsequent analysis of its absorbing and fluorescing properties can provide key insight into the dynamics of organic matter cycling in estuaries and coastal systems. For example, BEPOM fluorescence was modeled from samples collected in the NRE before and after a Category 1 hurricane and showed a distinct change in quality from autochthonous, plankton-derived OM to allochthonous, soil-derived OM (Osburn et al. 2012). Here, we focus our discussion on the structure in BEPOM absorption and explore the application of CDOM absorption parameters (e.g., spectral slope coefficients) to BEPOM. In addition, in situ data and BEPOM optical and geochemical data were used in a multivariate principal components analysis (PCA) to further explain BEPOM source and corresponding trends in coastal environments.

Absorption parameter trends

The typical absorption spectrum of CDOM in estuaries and coastal waters exhibits featureless exponential decay with increasing wavelength (Coble 2007). For most of the absorption spectra of BEPOM measured from the three different estuarine and coastal environments in this study, structure was observed in the form of broad peaks, centered around 280 nm and around 400 nm, in all three systems (Fig. 2; Fig. 3). The nature of these peaks is unknown, but very likely due to substituted aromatic compounds. The steeply decreasing BEPOM absorption bore remarkable resemblance to CDOM absorption spectra measured on cultures of *Trichodesmium spp*., and of mesoplankton ranging from copepods to salps and worms (Steinberg et al. 2004; Urban-Rich et al. 2006; Ortega-Reteurta et al. 2009).

While EEMs of BEPOM at freshwater stations formed patterns typical of terrestrial CDOM, a three distinct peak pattern representing tryptophan and NADH was associated with individual EEMs downstream and offshore (Fig. 12). This three peak pattern was consistently identified in samples with strong peaks in the corresponding absorption spectra.

High absorption and low spectral slope values reflect high molecular weight terrestrial humic substances in CDOM (Coble 2007). In many coastal environments, absorption values tend to decrease and spectra slope values increase along a salinity gradient, reflecting the dilution of high molecular weight compounds with low molecular weight compounds in seawater (Twardowski et al. 2004; Fichot and Benner 2012). BEPOM does not behave in a similar manner. In this study, absorption intensities were found to vary with site location, seasonality, and depth (Fig. 2; Fig. 3). No distinct trend emerged between these three factors and the corresponding BEPOM absorption spectra although $S_{275\text{-}295}$ increased with salinity.

The manner in which BEPOM $S_{275\text{-}295}$ and S_R values increased along a salinity gradient in this study was greater than corresponding values for CDOM in the Delaware estuary (Helms et al. 2008). This created two issues when interpreting BEPOM S_R values and attempting to compare results between BEPOM and CDOM. The first issue deals with understanding why S_R values increase along a salinity gradient. The increase in CDOM S_R values with salinity commonly observed in estuaries reflect either: 1) mixing between two end members having different S_R values; or 2) a loss of high molecular weight terrestrial humic-like compounds as they are converted into low molecular weight compounds via

photochemical or microbial degradation (Helms et al. 2008). BEPOM has a third possible situation: the presence of a substance or substances that strongly absorb in the UV-B and result in a very steep slope for $S_{275\text{-}295}$. The larger S_R values for BEPOM implies a greater abundance of low molecular weight compounds in the particulate fraction that is extractable into base as opposed to the dissolved phase. This would appear to be in conflict with published geochemical studies identifying a greater amount of high molecular weight compounds in POM than in DOM (Gochin et al. 1994; Volkman and Tanoue 2002). However, the reason for the increase in values of $S_{275\text{-}295}$ and thus S_R that we observed in these estuaries is purely caused by the presence of the broad peak absorption at 260±20 nm. The strength of the peak signal causes an increase in absorption that, when log-linearized, produces a distinctly steeper slope from 275-295 nm. Removing the broad UV-B peak produced generally lower S_R values that fell in the range closer to that previously reported for CDOM (Fig. 5a; e.g., Helms et al. 2008).

The second issue is whether there was a disconnect in the information obtained from S_R regarding OM quality in POM versus DOM. CDOM S_R values can be expressed as a degradation index for terrestrial OM. Unless there is an addition of fresh terrestrial OM from tributaries within a system, S_R values increase conservatively along a salinity gradient during coastal mixing between freshwater and seawater (Helms et al. 2008). BEPOM S_R values do not behave like CDOM S_R values because primary production, in addition to other factors that drive CDOM S_R values (e.g. photobleaching and/or microbial degradation), has a stronger influence on BEPOM. Therefore, it is hypothesized that alkaline extraction

preferentially solubilizes non-humic, but light absorbing and fluorescing biological molecules into solution.

Tryptophan exhibits peak absorption at 280 nm and is likely the source of the peak we observe in BEPOM spectra near 280 nm (Lakowicz 2009). Previous research on the extraction and measurement of mycosporine amino acids absorbance spectra identified peaks around 320-390 nm (Whitehead and Vernet 2000). These compounds could contribute to the secondary BEPOM absorption peaks from 350-400 nm observed in some NRE samples (Fig. 2). It is likely that BEPOM S_R values are driven by fresh biological molecules related to primary production, indicating that BEPOM S_R values provide information distinct from CDOM S_R values. Potential candidates are the aforementioned tryptophan, as well as chlorinated carboxylic acids and ubiquinone, the latter was a predominant feature of the BEPOM EEM fluorescence (Fig. 12; Repeta et al. 2004; Cory and McKnight 2005). As indicated in Fig. 2, the intensity of the broad peaks in the BEPOM absorption spectra of mid-estuarine stations in the NRE was intermittent, but it did appear to be a feature of stations likely more influenced by recent primary production (Fig. 8b).

Analysis of BEPOM absorption post removal of spectra shape

Removing the peaks in BEPOM absorption spectra around 280 nm had minimal benefit in attaining qualitative information from S_R. Low absorption between 350-400 nm resulted in poor non-linear fit on the excluded data for some samples and artificially high S_R values (GOM St. 2 surface, pre S_R=3.49, post S_R=2.00). $S_{275-295}$ calculated separately on the original and peak-corrected absorption values were positively related (R^2=0.94; Fig. 5b).

The scattering of $S_{275-295}$ values about the regression line was the same for the post-corrected values and the original data (R^2=0.72; Fig. 5a). Fichot and Benner (2012) identified a strong nonlinear relationship between $S_{275-295}$ and DOC-normalized lignin yield in surface waters in the northern GOM, Mississippi River, and Atchafalaya River, indicating $S_{275-295}$ as a tracer for percent terrigenous DOC in river dominated systems. This was not observed in the particulate fraction; while NRE BEPOM $S_{275-295}$ values increased with salinity, BEPOC concentrations were greatest in mid-estuary as was chlorophyll concentrations supporting the hypothesis that BEPOM is biologically influenced.

NCG-PARAFAC model and PCA analysis

The BEPOM absorption data strongly suggested the influence of recent biological activity in BEPOM. Our fluorescence results and PCA models provided a more robust understanding of BEPOM sources, including the NADH/ubiquinone-like component 1 which explained the most variability in the data set. Component 6 was unique to the NCG-PARAFAC model. Observations of Fmax intensities from individual samples identified GOM bottom water as the primary source of component 6 reflecting potential re-suspension of humic material (Fig. 9). The observation of increased humic material in oceanic bottom water has been observed in CDOM globally (Jørgensen et al. 2011). Although, it should be noted that in this study, increased concentrations of marine humic substances such as component 6 in BEPOM was not observed at all open water stations.

PCA models were also included, explaining relationships of BEPOM geochemical proxies and in situ measurements to absorbance and fluorescence data. One PCA model

included Fmax values for each component, dissolved oxygen (DO), salinity, $S_{275-295}$ and chlorophyll a data from all three systems (Fig. 10). The second model included the previously mentioned parameters in addition to geochemical parameters: BEPOC concentrations, δ^{13}C-BEPOM, and C:N of the total POM. However, since this additional geochemical data was available only for the NRE, the second model only included samples from the NRE (Fig. 11).

Each PCA model explained 60-65% of the total variance. Salinity was represented as PC1; NADH-like component 1 trended with salinity while the allochthonous components 2 and 4 trended negatively with salinity, for both models. The strongest evidence for the change in POM quality tracked by BEPOM fluorescents is seen in the NRE-PCA. In the NRE-PCA model, chlorophyll a trended positively with BEPOC concentration and δ^{13}C-BEPOM values. It is likely that PC2 in the NRE-PCA model represents an index of degradation in BEPOM as C:N ratios trend opposite of components 1 and 5, reflecting nitrogen enrichment in POM.

TCC analysis for POM-DOM cycling

The NCG-PARAFAC model was compared to a PARAFAC model fit separately on POM and DOM EEMs from the NRE (Osburn et al. 2012; Fig. A.1). Tucker's congruence coefficient (TCC) was used to compare the factor similarity of the two PARAFAC models, each having six components (Lorenzo-Seva and Berge 2006). This analysis was used to determine which components were similar between the two models, rather than determining if the models were the same (Stedmon and Bro 2008). The output of the test was a matrix,

TCC, where the rows of TCC correspond to the components in the Osburn NRE-PARAFAC model and the columns of TCC correspond to the components in the NCG-PARAFAC model from this study (Table 4). A value of 1 indicated that the excitation and emission loadings were not significantly different ($p<0.05$), whereas a value of 0 indicated a significant difference. Based on this test, four of the six components in either model were similar. The NCG-PARAFAC component 4 was not significantly different from components 2 and 3 in the Osburn NRE-PARAFAC model. Component 4 fluoresces in the humic region and based on its PCA scores, appears to be a marker for allochthonous OM (Fig. 10; Fig. 11). Component 5 of the NCG-PARAFAC model did not match any of the components from the Osburn NRE-PARAFAC model. This component does, however, strongly resemble marine (or rather microbial) humic fluorescence first observed by Coble (1993) in a study of XAD isolates of seawater, but later observed in many aquatic ecosystems, and specifically related to recent biological production (Fellman et al. 2010).

It was striking that PARAFAC components from three very different environments were statistically similar. Thus, PARAFAC models calculated on different estuarine and coastal ecosystems can provide information regarding distinct characteristics that would otherwise not be modeled while focusing on one ecosystem. This result extends the utility of PARAFAC to capture a wide range of variability in OM fluorescence across estuaries and coastal waters.

CONCLUSION

The aim of this study was to apply the BEPOM method to three different coastal environments and to compare the results of BEPOM optical properties as a means of evaluating POM quality across the terrestrial-marine continuum. While S_R values for BEPOM were informative, the influence of peaks, presumably related to autochthonous production, added structure to absorption spectra, and resulted in S_R values much higher than commonly observed for estuarine CDOM which typically exhibit featureless exponential decay that can be modeled with a single exponential term. However, it was determined in this work that the presence of the peaks resulted in S_R values that behaved similarly to BEPOM absorption spectra with the peak removed. Therefore, further research into the compounds causing the absorption peak is warranted for they could provide a unique tracer for a precursor to autochthonous or planktonic CDOM. For example, future work could investigate the spectral similarity between samples having BEPOM absorption peaks, as we have measured in this study, and chemical compounds such as chlorinated biphenyls, which appear to be markers for marine phytoplankton (Repeta et al. 2004). Future work on understanding CDOM production by plankton should incorporate the BEPOM approach because of the similarity between BEPOM absorption spectra shown in this study and the absorption produced by mesoplankton in culture (Steinberg et al. 2004). BEPOM may also provide insight into the optical properties of the sea surface microlayer and the poorly understood carbon cycling that occurs in this dynamic interface between the oceans and the atmosphere (Orellana and Verdugo 2003; Ortega-Retuerta et al. 2009).

The utility of BEPOM optical properties requires some caution when making direct comparisons to CDOM. In photodegradation experiments, S_R values of unfiltered Neuse River water increased to values that mimic photodegradation of CDOM in offshore, coastal waters (Osburn et al. 2012). Thus, direct comparison of BEPOM S_R value to a corresponding CDOM S_R value should be made with caution. Instead $S_{275\text{-}295}$ values should be used on any future BEPOM absorbance studies. However, our results suggest that the slope is not an exclusive tracer for terrigenous OM in coastal waters as may be the case for CDOM (Fichot and Benner 2012).

A PARAFAC model containing six components was fit to BEPOM solutions extracted from POM across the three environments studied. This model revealed several autochthonous sources in BEPOM and only two which exhibited strong resemblance to humic substances. Comparing the model statistically to a separate PARAFAC model fit on previously published CDOM and BEPOM samples from the NRE confirmed that the POM base extraction technique is capturing similar information among different estuarine and coastal ecosystems.

Finally, absorption and fluorescence information in this study was validated by geochemical information. BEPOC and stable C isotope values of BEPOM provided important context with which to interpret the optical information. This offers a potential for application of optical properties to investigate POM dynamics in water columns and possibly, also in sediments. Multivariate statistical modeling captured the majority of variation in POM chemical and optical measurements in this unique data set. These results

provide compelling support for plankton sources of CDOM in coastal waters. Further work is warranted to compare the chemical and photophysical properties of BEPOM to *de facto* terrestrial models (e.g., the electronic interaction model proposed by Del Vecchio and Blough 2004). This study has demonstrated the BEPOM technique as a means of understanding POM cycling in estuaries and coastal environments.

FIGURES

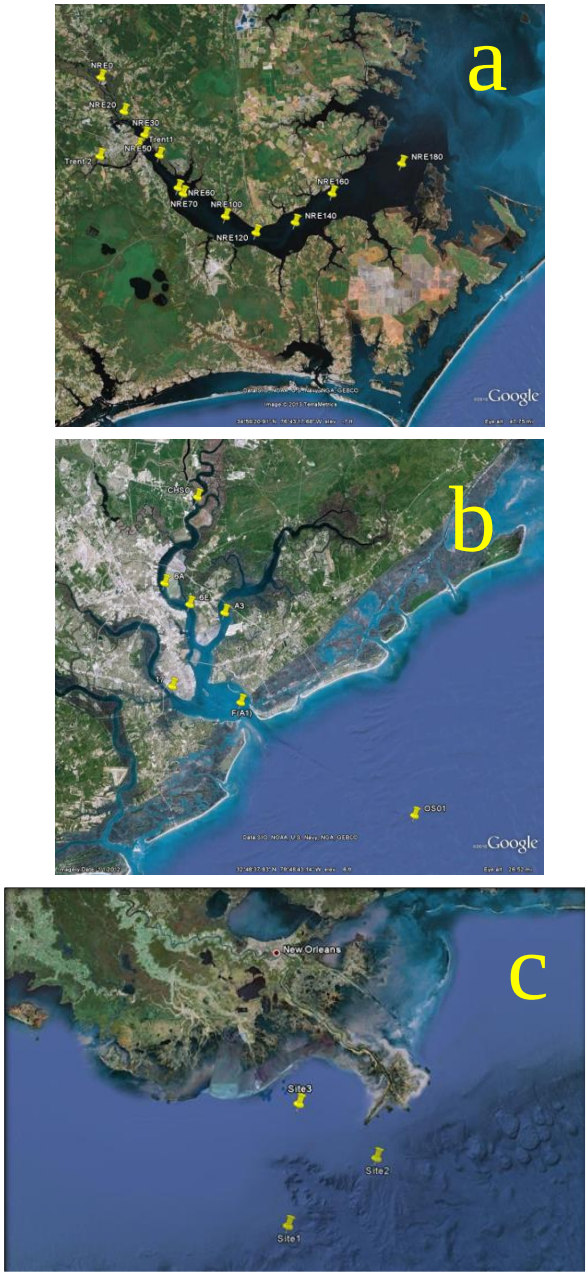

Figure 1: Study area and sampling stations. (a) Neuse River Estuary (NRE) stations 0-180 and Trent River stations (T1 and T2). (b) Charleston Harbor (CHS) stations A3 in the Wando River; CHS0, 6A, 6E in the Cooper River; 17 in the Ashley River; the salinity front (F) at the harbor mouth; OS01 offshore on the inner shelf of the South Atlantic Bight. (c) Gulf of Mexico (GOM) stations 01, 02 and 03.

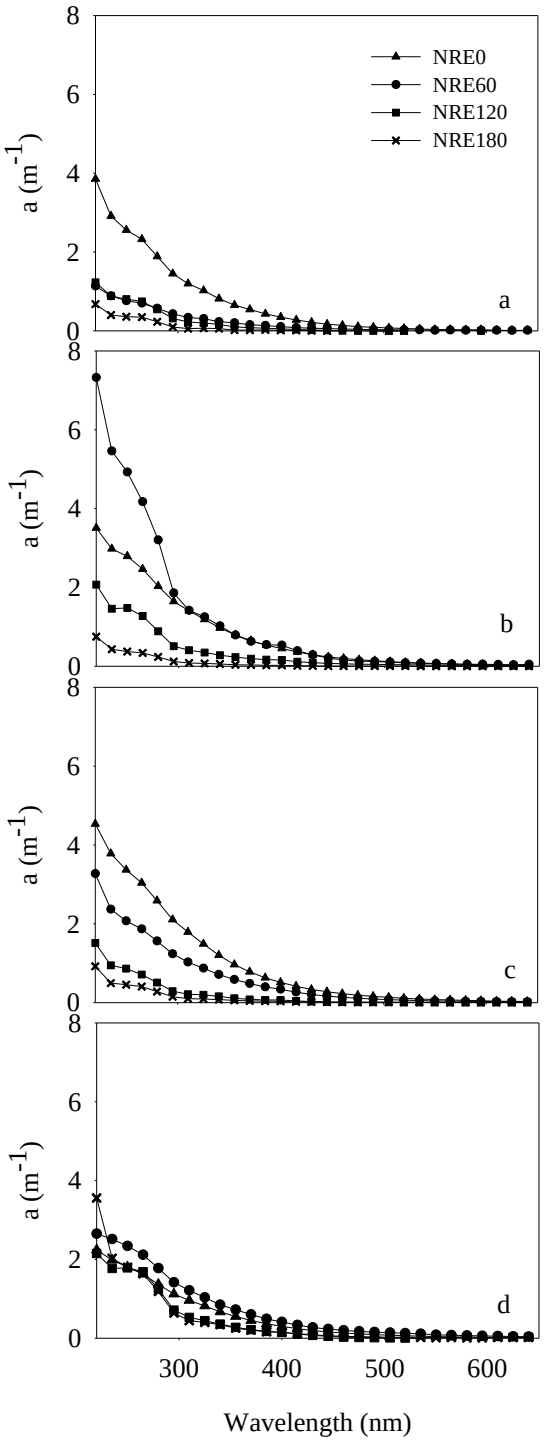

Figure 2: Corrected BEPOM absorption spectra for the NRE in (a) September 2011, (b) February 2012, (c) March 2012, and (d) September 2012. Stations included are NRE0 (triangles), NRE60 (circles), NRE120 (squares), and NRE180 (x's).

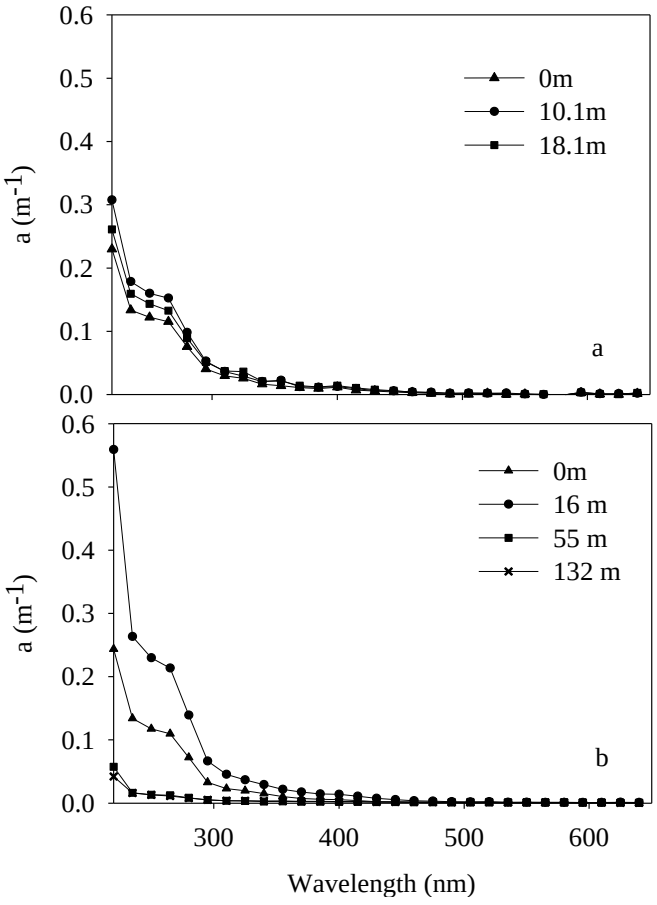

Figure 3: Changes in BEPOM absorption spectra with depth for (a) Station OS01 in the South Atlantic Bight and (b) Station 2 in the northern Gulf of Mexico.

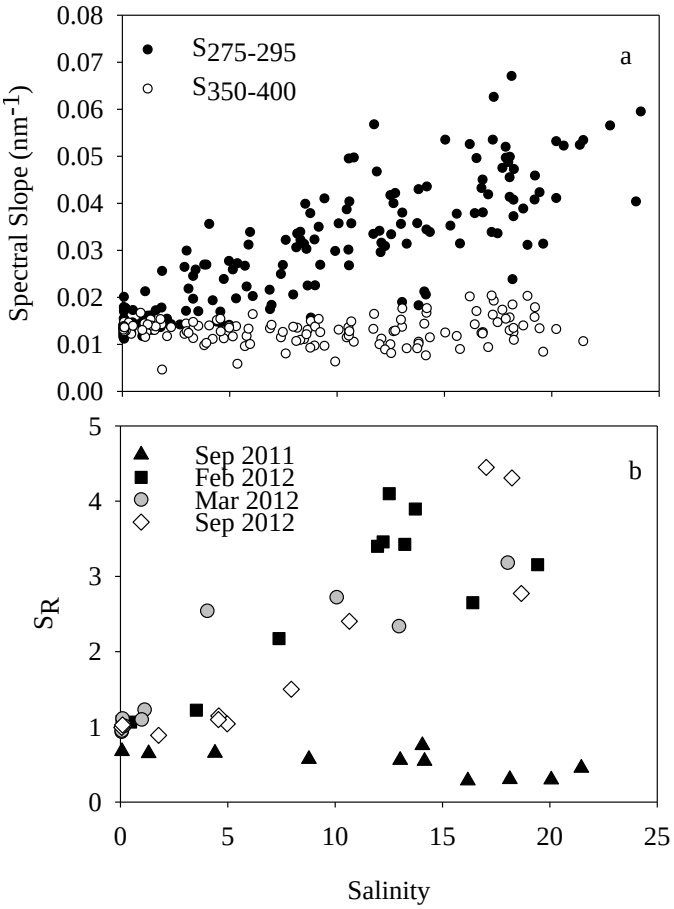

Figure 4: Salinity plotted against (a) BEPOM $S_{275\text{-}295}$ (filled circles) and $S_{350\text{-}400}$ (open circles) for all NRE samples and (b) S_R for September 2011 (filled triangles), February 2012 (filled squares), March 2012 (filled circles), and September 2012 (open diamonds).

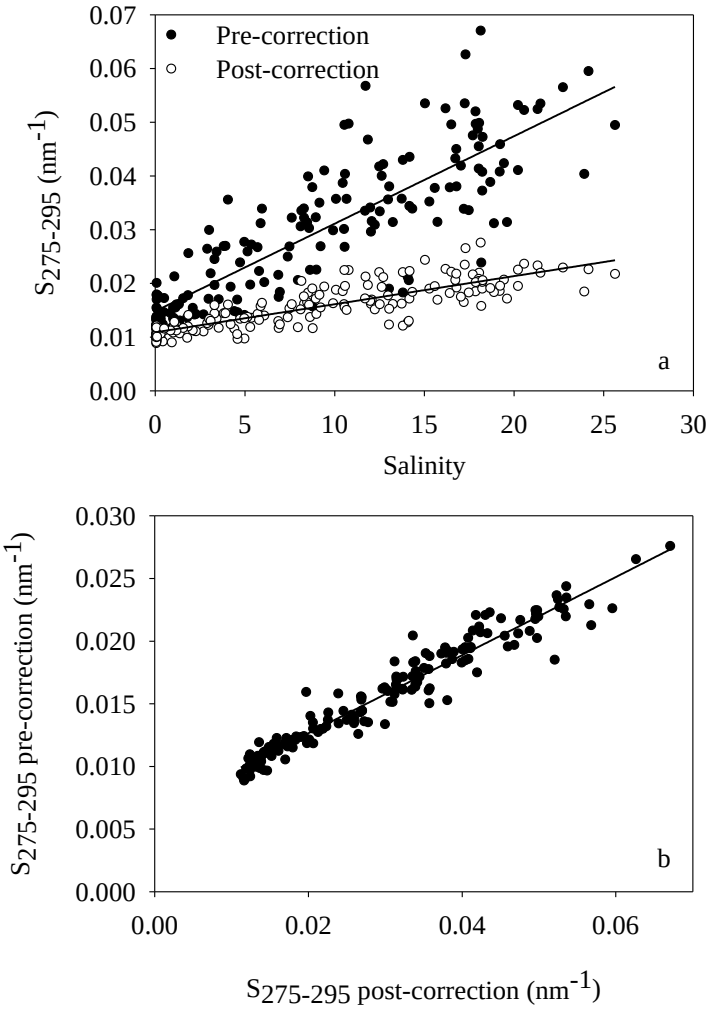

Figure 5: Comparison of BEPOM $S_{275-295}$ pre and post removal of spectra peak around 285 nm against (a) salinity, and (b) pre and post-correction.

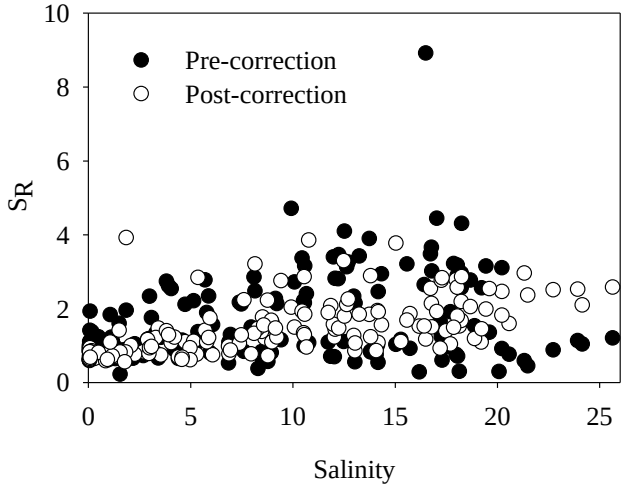

Figure 6: Slope Ratio pre (filled circles) and post (open circles) removal of the broad spectral peak around 285 nm, prevalent in BEPOM absorption, for all NRE samples.

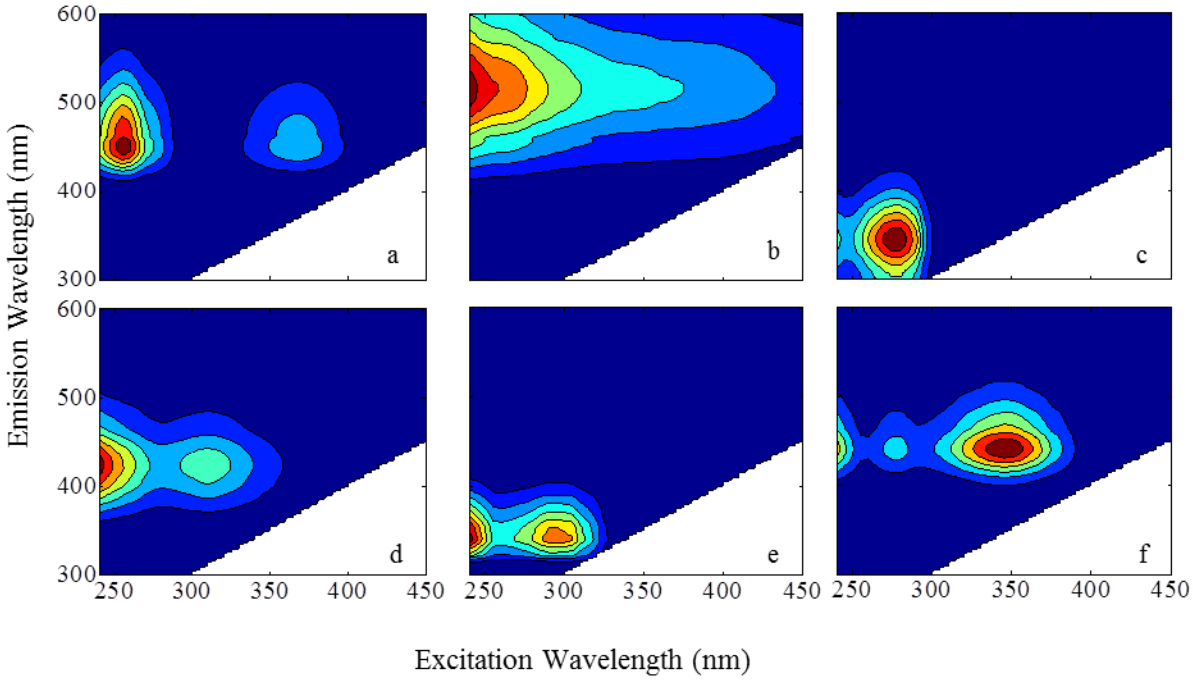

Figure 7: Results of a PARAFAC model fit to all BEPOM EEMs in this study. Contour plots of each split-half validated component 1-6 in the NCG-PARAFAC model are labeled a, b, c, d, e, and f, respectively.

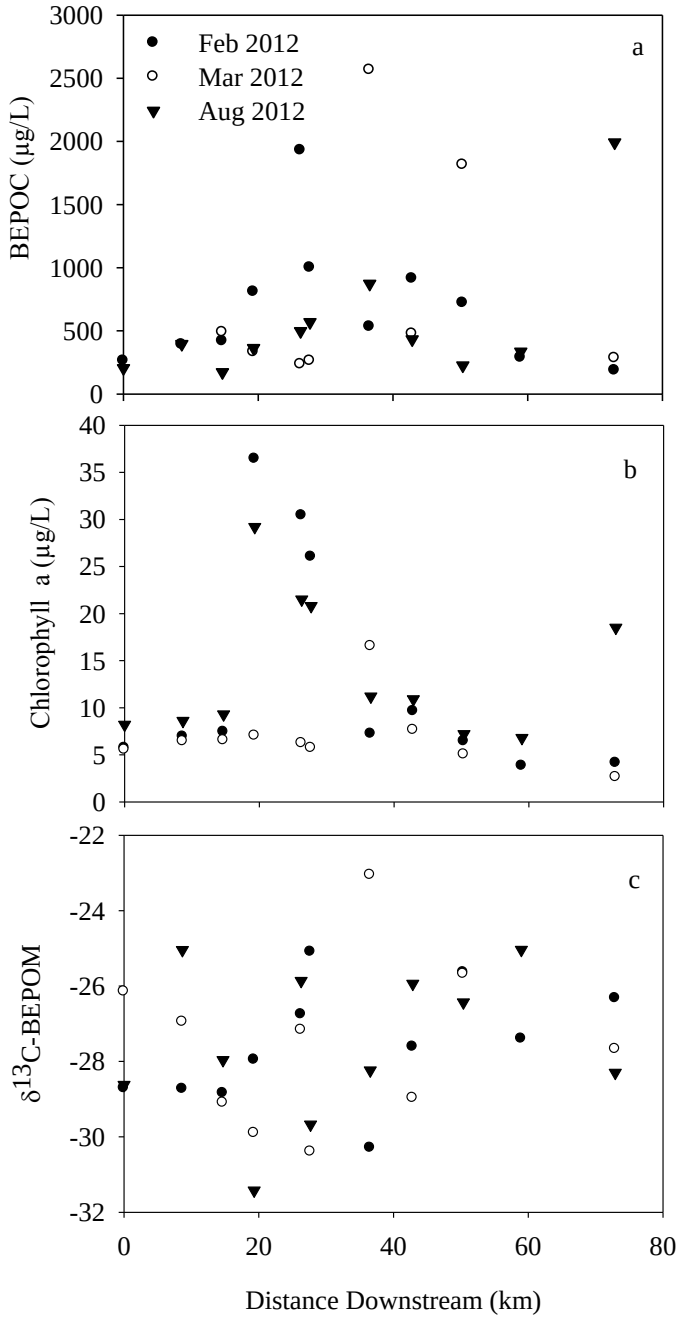

Figure 8: Neuse River Estuary values for (a) BEPOC, (b) Chlorophyll a and (c) δ^{13}C-BEPOM in February (filled circles), March (open circles), and August (filled triangles) 2012. Each parameter was plotted against the distance downstream from NRE0 (nominally, the freshwater riverine reach of the estuary).

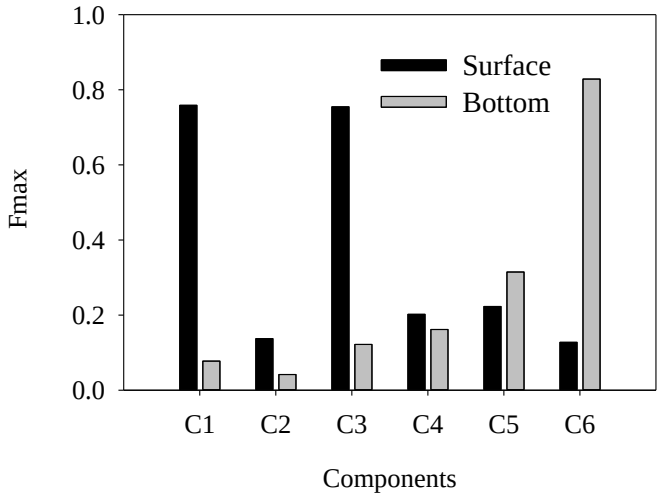

Figure 9: Fmax for each component from the NCG-PARAFAC model for surface (black) and bottom (gray) waters from GOM Sta. 01.

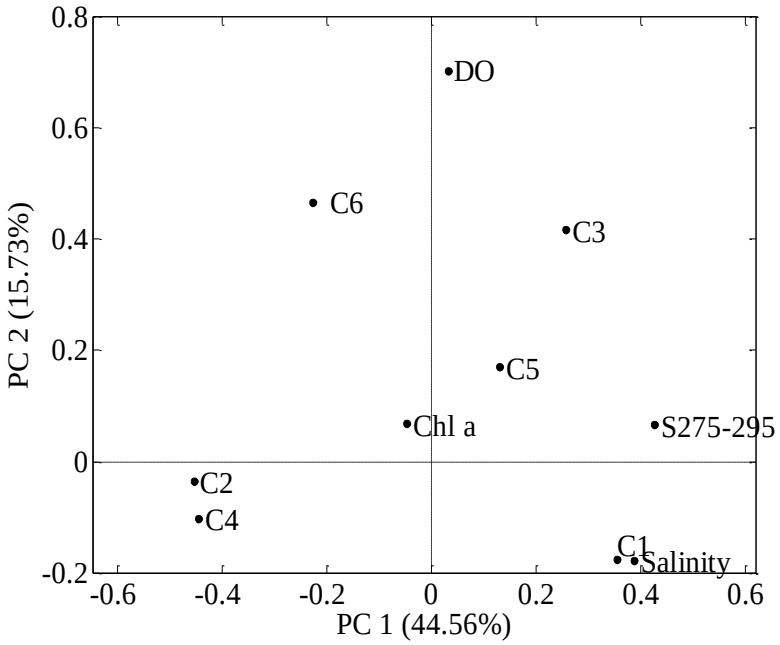

Figure 10: PCA model on optical properties and in situ measurements from the NRE, CHS, and GOM (n=204). PC1 explained 44.56% of the variation in the data, while PC2 explained 15.73%.

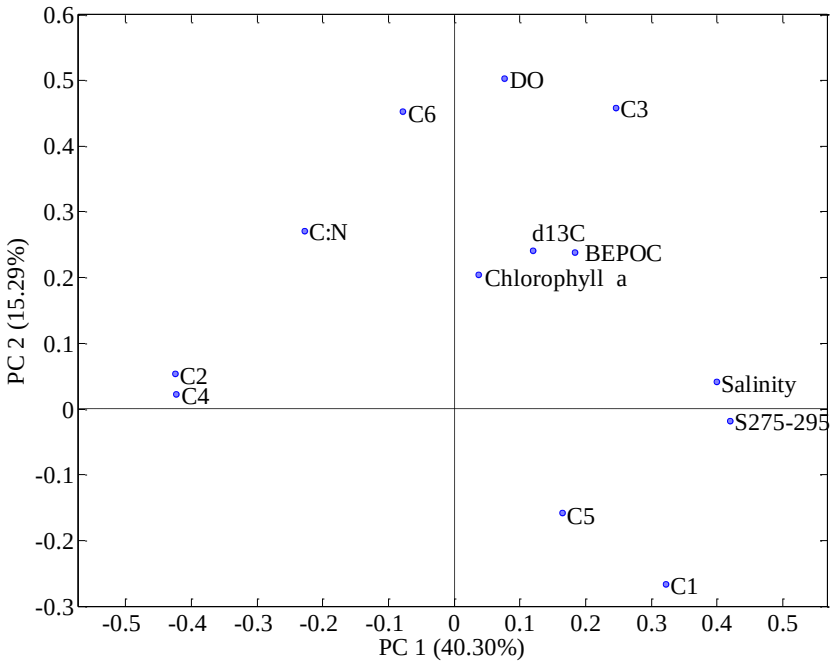

Figure 11: PCA model of optics, in situ measurements, and geochemical proxies from NRE samples (n=64). PC1 explained 40.3% of the variation in the data, while PC2 explained 15.29%.

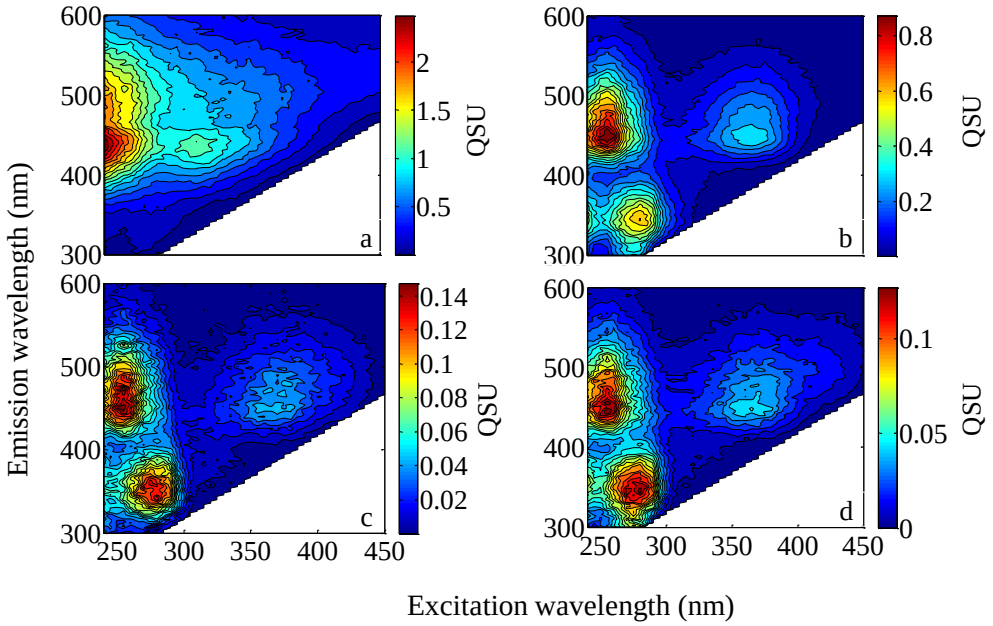

Figure 12: Examples of individual EEM patterns from surface samples at (a) NRE0 in March 2012, (b) NRE180 in March 2012, (c) CHS offshore, and (d) GOM station 2.

TABLES

Table 1: Study site, latitude and longitude, depth, spectral parameters ($S_{275-295}$, Fmax components 1-6), and in situ measurements (D.O, chlorophyll, salinity). GOM stations include Sta.1, 2, 3. CHS stations include A3, OS01, Fronts (F) F01, F07, F13, CHS0, 6E, CHS17, and 6A; depth and nepheloid layer (NP). Monthly averages were calculated for all NRE stations.

Site	Latitude	Longitude	Depth (m)	Distance Downstream (km)	Salinity	Chlorophyll a (µg/L)	DO (mg/L)	$S_{275-295}$	C1	C2	C3	C4	C5	C6
GOM														
Station 1	28.2	-89.6	1	-	30.9	0.7	4.49	0.045	0.759	0.138	0.755	0.202	0.223	0.128
			10	-	31.3	0.6	4.50	0.044	0.687	0.137	0.729	0.197	0.359	0.187
			70	-	36.4	0.2	3.69	0.041	0.000	0.007	0.043	0.009	0.092	0.894
			111	-	36.4	0.1	2.77	0.032	0.078	0.042	0.122	0.162	0.315	0.829
Station 2	28.4	-89.2	1	-	33.0	1.2	4.48	0.051	0.809	0.143	0.892	0.196	0.136	0.035
			16	-	35.1	1.2	3.62	0.049	0.253	0.088	0.859	0.159	0.167	0.025
			55	-	36.4	0.2	3.83	0.036	0.413	0.123	0.533	0.369	0.207	0.013
			132	-	36.3	0.1	2.69	0.030	0.373	0.147	0.344	0.364	0.122	0.010
Station 3	28.6	-89.6	1	-	30.1	1.7	4.30	0.054	0.232	0.061	0.923	0.198	0.104	0.000
			19	-	34.1	0.6	4.09	0.052	0.287	0.067	0.870	0.182	0.178	0.000
			125	-	36.3	0.1	2.76	0.045	0.395	0.100	0.250	0.231	0.333	0.000
CHS														
A3	32.8	-79.9	1.3	-	23.3	13.6	4.70	0.048	0.691	0.130	0.363	0.273	0.137	0.030
			13.3	-	24.8	10.0	4.64	0.047	0.747	0.155	0.486	0.347	0.150	0.021
			11.8	-	28.8	8.8	4.56	0.033	0.647	0.129	0.621	0.317	0.245	0.015
			NP	-	28.8	46.6	4.56	0.026	0.479	0.313	0.343	0.609	0.193	0.058
OS01	32.7	-79.7	6.3	-	35.9	1.6	1.24	0.043	0.863	0.100	0.506	0.125	0.139	0.000
			10.1	-	36.0	1.6	1.16	0.043	0.846	0.109	0.698	0.171	0.208	0.000
			18.1	-	36.0	1.6	0.94	0.037	0.922	0.092	0.343	0.117	0.129	0.000
CHS F01	32.8	-79.9	-	-	25.8	10.8	4.61	0.027	0.785	0.099	0.639	0.233	0.127	0.008
CHS F07			-	-	24.6	8.7	4.66	0.043	0.780	0.071	0.422	0.213	0.076	0.000
CHS F13			-	-	25.0	8.5	4.64	0.034	0.734	0.096	0.528	0.230	0.104	0.007
CHS0	32.9	-79.9	0.9	-	5.6	3.0	5.07	0.016	0.598	0.256	0.523	0.452	0.151	0.062
			2.8	-	6.5	6.0	5.05	0.012	0.469	0.343	0.294	0.599	0.159	0.082
			5.5	-	10.4	6.7	4.99	0.012	0.419	0.332	0.320	0.633	0.168	0.083
6E	32.8	-79.9	1	-	17.1	19.8	4.78	0.017	0.823	0.132	0.592	0.261	0.131	0.045
			2.6	-	23.0	10.5	4.69	0.020	0.699	0.093	0.521	0.237	0.077	0.012
			6.9	-	28.0	8.0	4.57	0.019	0.711	0.094	0.716	0.274	0.115	0.011
			NP	-	28.0	42.4	4.57	0.015	0.490	0.267	0.298	0.614	0.156	0.057
CHS17	32.8	-80.0	1.5	-	25.6	12.2	4.58	0.019	0.584	0.092	0.500	0.432	0.141	0.083
			5.4	-	25.8	12.8	4.58	0.016	0.567	0.126	0.616	0.472	0.129	0.087
6A	32.9	-80.0	1.3	-	13.9	4.8	4.95	0.026	0.664	0.137	0.428	0.323	0.081	0.019
			11.8	-	28.5	6.4	4.55	0.021	0.647	0.137	0.498	0.362	0.083	0.017
			13.3	-	28.5	5.6	4.56	0.038	0.671	0.124	0.421	0.388	0.123	0.013
			NP	-	28.5	9.7	4.55	0.039	0.591	0.169	0.321	0.415	0.126	0.021
NRE Yearly Averages														
Trent 1	35.1	-77.0	0.2	-	2.9	9.8	7.03	0.020	0.279	0.386	0.325	0.576	0.152	0.095
Trent 2	35.1	-77.1	0.2	-	2.2	10.3	6.17	0.017	0.235	0.471	0.375	0.593	0.115	0.094
NRE 0	35.2	-77.1	0.2	0.0	0.1	7.2	6.20	0.012	0.217	0.477	0.117	0.698	0.083	0.085
NRE 20	35.2	-77.1	0.2	8.7	0.9	11.4	5.95	0.016	0.209	0.442	0.195	0.671	0.102	0.075
NRE 30	35.1	-77.0	0.2	14.7	2.9	9.2	7.16	0.017	0.360	0.348	0.200	0.602	0.080	0.078
NRE 50	35.1	-77.0	0.2	19.3	4.7	15.1	7.39	0.021	0.340	0.318	0.364	0.529	0.161	0.075
NRE 60	35.0	-77.0	0.2	26.3	7.2	14.3	8.37	0.026	0.421	0.254	0.393	0.451	0.124	0.076
NRE 70	35.0	-77.0	0.2	27.7	8.1	12.5	8.71	0.027	0.444	0.252	0.425	0.443	0.122	0.074
NRE 100	35.0	-76.9	0.2	36.6	10.9	11.2	8.58	0.033	0.532	0.177	0.513	0.337	0.147	0.076
NRE 120	34.9	-76.8	0.2	42.9	12.2	11.4	8.50	0.035	0.553	0.138	0.577	0.274	0.173	0.067
NRE 140	35.0	-76.7	0.2	50.4	15.6	8.0	8.01	0.041	0.657	0.115	0.585	0.229	0.148	0.075
NRE 160	35.0	-76.7	0.2	59.0	17.9	8.7	7.44	0.040	0.598	0.087	0.591	0.184	0.223	0.072
NRE 180	35.1	-76.5	0.2	72.9	19.6	9.7	7.93	0.042	0.632	0.096	0.577	0.182	0.179	0.062

Table 2: Excitation and emission wavelength(s) of corresponding components from the NRE-PARAFAC model and the NCG-PARAFAC model.

Ex/Em	NRE	NCG
250 (360)/440	C4	C1
240/500	C2	C2
270/330	C1	C3
245 (305)/416	C3	C4
240 (285)/334	C5	C5
240 (335)/430	-	C6

Table 3: NRE monthly station averages of BEPOC, stable carbon isotope, atomic ratio of carbon to nitrogen from the total organic carbon concentration, and extraction efficiency of base extracted organic carbon to total organic carbon between August 2011-September 2012. δ^{13}C-DIC values were collected in May 2013.

Station	BEPOC (µg/L)	BEPOC Standard Deviation	δ^{13}C-BEPOM (‰)	δ^{13}C-BEPOM Standard Deviation	C:N	OC Extraction Efficiency (%)	δ^{13}C-DIC PDB*
Trent 1	433	338	-28.22	0.97	-	-	-
Trent 2	303	123	-28.76	1.23	-	-	-
NRE 0	481	590	-27.30	2.39	9.87	44.0	-13.44
NRE 20	643	651	-28.07	2.75	7.88	34.7	-13.89
NRE 30	315	114	-29.40	1.63	10.21	36.6	-12.66
NRE 50	533	385	-30.55	2.58	8.82	43.5	-10.13
NRE 60	742	677	-27.14	0.99	8.62	28.3	-6.73
NRE 70	449	261	-27.83	2.07	9.31	22.4	-6.47
NRE 100	712	736	-26.95	2.41	8.38	34.3	-4.74
NRE 120	696	483	-28.00	2.23	7.96	35.7	-4.08
NRE 140	629	564	-26.51	2.07	7.80	40.7	-3.62
NRE 160	340	186	-27.54	3.34	7.89	24.9	-3.16
NRE 180	806	1056	-28.31	1.67	9.20	23.1	-2.11

Table 4: Tucker's congruence coefficient matrix (TCC). Columns are components 1-6 from the NCG-PARAFAC model created for this study. Rows are components 1-6 from the NRE-POM/DOM PARAFAC model created in Osburn et al (2012).

		NCG-PARAFAC Model					
NRE DOM-POM PARAFAC Model		C1	C2	C3	C4	C5	C6
	C1	0	1	0	0	0	0
	C2	0	0	0	1	0	0
	C3	0	0	0	1	0	0
	C4	1	0	0	0	0	0
	C5	0	0	1	0	0	0
	C6	0	0	0	0	0	1

REFERENCES

Arar, E. 1997. Method 446. In Vitro Determination of Chlorophylls a, b, c1+c2 and Pheopigments in Marine and Freshwater Algae by Visible Spectrophotometry. EPA, Ohio, USA.

Bricaud A, Morel A, Prieur L. 1981. Absorption by dissolved organic-matter of the sea (yellow substance) in the uv and visible domains. Limnol. Oceanogr. **26**:43-53.

Bro R. 1997. PARAFAC. tutorial and applications. Chemometrics Intellig. Lab Syst. **38**:149-71.

Burkholder JM, Dickey DA, Kinder CA, Reed RE, Mallin MA, McIver MR, Cahoon LB, Melia G, Brownie C, Smith J, et al. 2006. Comprehensive trend analysis of nutrients and related variables in a large eutrophic estuary: A decadal study of anthropogenic and climatic influences. Limnol Oceanogr. **51**:463-87.

Coble PG. 2007. Marine optical biogeochemistry: The chemistry of ocean color. Chem Rev. **107**:402-18.

Coble PG, Schultz CA, Mopper K. 1993. Fluorescence contouring analysis of DOC intercalibration experiment samples: A comparison of techniques. Mar Chem. **41**:173-8.

Cory, R. M. and D. M. McKnight. 2005. Fluorescence spectroscopy reveals ubiquitous presence of oxidized and reduced quinones in dissolved organic matter. Environ. Sci. Technol. **39**:8142-8149.

Del Vecchio R and Blough N. 2002. Photobleaching of chromophoric dissolved organic matter in natural waters: Kinetics and modeling. Mar. Chem. **78**:231-53.

Fellman JB, Petrone KC, Grierson PF. 2011. Source, biogeochemical cycling, and fluorescence characteristics of dissolved organic matter in an agro-urban estuary. Limnol. Oceanogr. **56**:243-56.

Fichot CG and Benner R. 2012. The spectral slope coefficient of chromophoric dissolved organic matter (S275-295) as a tracer of terrigenous dissolved organic carbon in river-influenced ocean margins. Limno.l Oceanogr. **57**:1453-66.

Golchin A, Oades J. Skjemstad J, Clarke P. 1994. Study of free and occluded particulate organic-matter in soils by solid-state C-13 Cp/mas nmr-spectroscopy and scanning electron-microscopy. Aust. J. Soil. Res. **32**:285-309.

Hargreaves, B.R. 2003. Water column optics and penetration of UVR, p. 59-99. *In* E. W. Helbling and H. Zagarese, H. [eds.], UV Effects in Aquatic Organism and Ecosystems. Academic.

Helms JR, Stubbins A, Ritchie JD, Minor EC, Kieber DJ, Mopper K. 2008. Absorption spectral slopes and slope ratios as indicators of molecular weight, source, and photobleaching of chromophoric dissolved organic matter. Limnol. Oceanogr. **53**:955-69.

Jerlov, Nils Gunnar. 1976. Marine optics, vol. 14. Elsevier Science.

Jørgensen L, Stedmon CA, Kragh T, Markager S, Middelboe M, Søndergaard M. 2011. Global trends in the fluorescence characteristics and distribution of marine dissolved organic matter. Mar. Chem. **126**:139-48.

Kowalczuk P, Durako MJ, Young H, Kahn AE, Cooper WJ, Gonsior M. 2009. Characterization of dissolved organic matter fluorescence in the south atlantic bight with use of PARAFAC model: Interannual variability. Mar. Chem. **113**:182-96.

Lakowicz, Joseph R., ed. 2009. Principles of fluorescence spectroscopy. 3rd edition. Springer.

Lawaetz AJ and Stedmon CA. 2009. Fluorescence intensity calibration using the raman scatter peak of water. Appl. Spectrosc. **63**:936-40.

Li W, Sheng G, Lu R, Yu H, Li Y, Harada H. 2011. Fluorescence spectral characteristics of the supernatants from an anaerobic hydrogen-producing bioreactor. Appl. Microbiol. Biotechnol. **89**:217-24.

Lorenzo-Seva, U., Berge, J.M.F.T. 2006. Tucker's congruence coefficient as a meaningful index of factor similarity. Methodology. **2**:57–64.

Matson E and Brinson M. 1990. Stable carbon isotopes and the C-N ratio in the estuaries of the pamlico and neuse rivers, north-carolina. Limnol. Oceanogr. **35**:1290-300.

Milliman J. 1991. Flux and fate of fluvial sediment and water in coastal seas, p. 513-564. *In* R. F. C. Mantoura, J. Martin, and R. Wollast [eds.], Ocean Margin Processes in Global Change. Academic.

Orellana M and Verdugo P. 2003. Ultraviolet radiation blocks the organic carbon exchange between the dissolved phase and the gel phase in the ocean. Limnol. Oceanogr. **48**:1618-23.

Ortega-Retuerta E, Frazer TK, Duarte CM, Ruiz-Halpern S, Tovar-Sanchez A, Arrieta JM, Reche I. 2009. Biogeneration of chromophoric dissolved organic matter by bacteria and krill in the southern ocean. Limnol. Oceanogr. **54**:1941-50.

Osburn CL and Stedmon CA. 2011. Linking the chemical and optical properties of dissolved organic matter in the baltic-north sea transition zone to differentiate three allochthonous inputs. Mar. Chem. **126**:281-94.

Osburn CL, Handsel LT, Mikan MP, Paerl HW, Montgomery MT. 2012. Fluorescence tracking of dissolved and particulate organic matter quality in a river-dominated estuary. Environ. Sci. Technol. **46**:8628-36.

Paerl H, Pinckney J, Fear J, Peierls B. 1998. Ecosystem responses to internal and watershed organic matter loading: Consequences for hypoxia in the eutrophying neuse river estuary, north carolina, USA. Mar. Ecol. Prog. Ser. **166**:17-25.

Pohlman J, Coffin R, Mitchell C, Montgomery M, Spargo B, Steele J, Boyd T. 2002. Transport, deposition and biodegradation of particle bound polycyclic aromatic hydrocarbons in a tidal basin of an industrial watershed. Environ. Monit. Assess. **75**:155-67.

Presley B, Trefry J, Shokes R. 1980. Heavy-metal inputs to mississippi delta sediments - a historical view. Water Air and Soil Pollution. **13**:481-94.

Repeta D, Hartman N, John S, Jones A, Goericke R. 2004. Structure elucidation and characterization of polychlorinated biphenyl carboxylic acids as major constituents of chromophoric dissolved organic matter in seawater. Environ. Sci. Technol. **38**:5373-8.

Rochelle-Newall EJ and Fisher TR. 2002. Production of chromophoric dissolved organic matter fluorescence in marine and estuarine environments: An investigation into the role of phytoplankton. Mar. Chem. **77**:7-21.

Romera-Castillo C, Sarmento H, Anton Alvarez-Salgado X, Gasol JM, Marrase C. 2011. Net production and consumption of fluorescent colored dissolved organic matter by natural bacterial assemblages growing on marine phytoplankton exudates. Appl. Environ. Microbiol. **77**:7490-8.

Romera-Castillo C, Sarmento H, Anton Alvarez-Salgado X, Gasol JM, Marrase C. 2010. Production of chromophoric dissolved organic matter by marine phytoplankton. Limnol. Oceanogr. **55**:446-54.

Santín C, Yamashita Y, Otero XL, Alvarez MA, Jaffe R. 2009. Characterizing humic substances from estuarine soils and sediments by excitation-emission matrix spectroscopy and parallel factor analysis. Biogeochemistry. **96**:131-47.

Senesi N, Miano TM, Provenzano MR, Brunetti G. 1989. Spectroscopic and compositional comparative characterization of I.H.S.S. reference and standard fulvic and humic acids of various origin. Sci. Total. Environ. **81–82**:143-56.

Sleighter RL and Hatcher PG. 2007. The application of electrospray ionization coupled to ultrahigh resolution mass spectrometry for the molecular characterization of natural organic matter. Journal of Mass. Spectrometry. **42**:559-74.

Stedmon, C.A. & Markager, S.S. 2003. Behaviour of the optical properties of coloured dissolved organic matter under conservative mixing. Est. Coast. Shelf Sci.**57**:973-979

Stedmon, C.A. & Markager, S.S. 2005. Tracing the production and degradation of autochthonous fractions of dissolved organic matter by fluorescence analysis. Limnol. Oceanogr. **50**: 1415-1426.

Stedmon C, Markager S, Bro R. 2003. Tracing dissolved organic matter in aquatic environments using a new approach to fluorescence spectroscopy. Mar. Chem. **82**:239-54.

Stedmon CA and Bro R. 2008. Characterizing dissolved organic matter fluorescence with parallel factor analysis: A tutorial. Limnology and Oceanography-Methods **6**:572-9.

Steinberg D, Nelson N, Carlson C, Prusak A. 2004. Production of chromophoric dissolved organic matter (CDOM) in the open ocean by zooplankton and the colonial cyanobacterium trichodesmium spp. Mar Ecol. Prog. Ser. **267**:45-56.

Stevenson FJ. 1994. Humus chemistry. Genesis, composition reactions, 2nd edn. Wiley.

Twardowski MS, Boss E, Sullivan JM, Donaghay PL. 2004. Modeling the spectral shape of absorption by chromophoric dissolved organic matter. Mar. Chem. **89**:69-88.

Urban-Rich, J., McCarty, J. T., Fernández, D., & Acuña, J. L. 2006. Larvaceans and copepods excrete fluorescent dissolved organic matter (FDOM). J. Exp. Mar. Biol. Ecol. **332**: 96-105.

Vahatalo A and Zepp R. 2005. Photochemical mineralization of dissolved organic nitrogen to ammonium in the baltic sea. Environ. Sci. Technol. **39**:6985-92.

Vernet M and Whitehead K. 1996. Release of ultraviolet-absorbing compounds by the red-tide dinoflagellate lingulodinium polyedra. Mar. Biol. **127**:35-44.

Volkman J and Tanoue E. 2002. Chemical and biological studies of particulate organic matter in the ocean. J. Oceanogr. **58**:265-79.

Wiegert, R. G., and B. J. Freeman. 1990. Tidal salt marshes of the southeast Atlantic Coast: A community profile. United States Fish and Wildlife Service Biological Report. **85**:1–67.

Whitehead K and Vernet M. 2000. Influence of mycosporine-like amino acids (MAAs) on UV absorption by particulate and dissolved organic matter in la jolla bay. Limnol. Oceanogr. **45**:1788-96.

APPENDIX
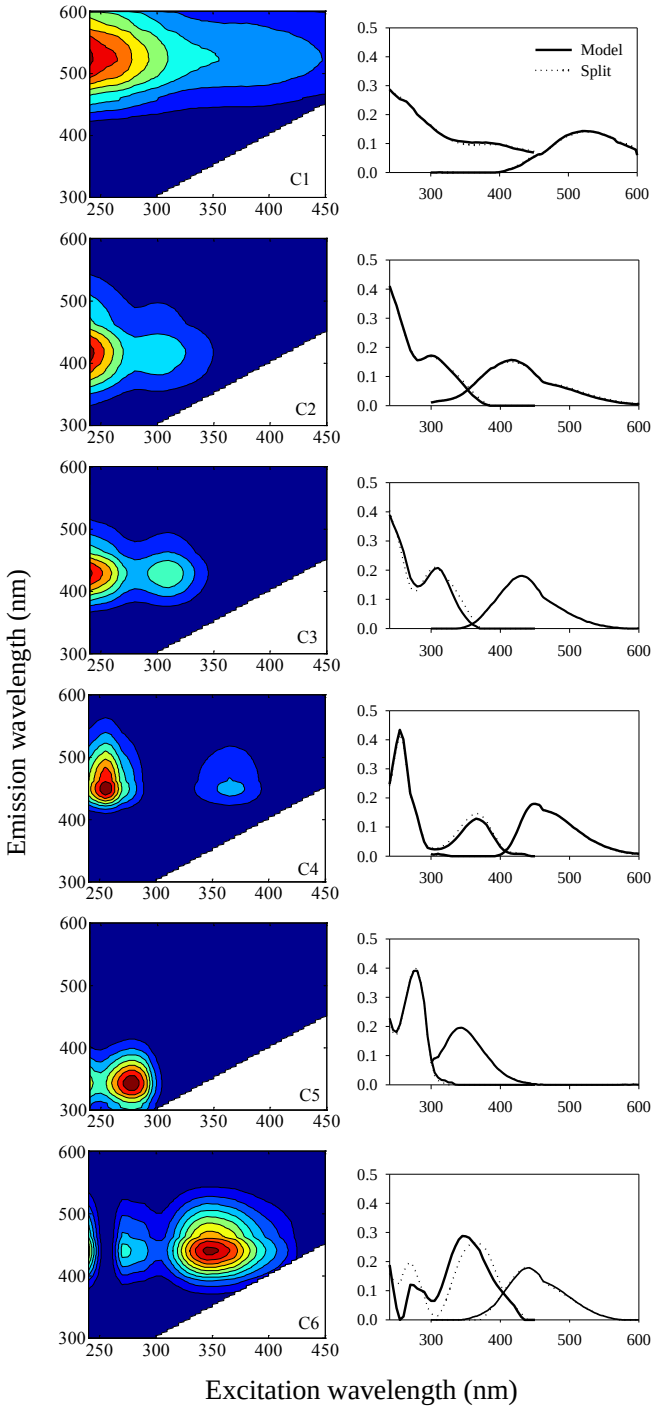
Appendix A: Loadings and leverages from the Osburn et al. (2012) NRE POM/DOM PARAFAC model.